# A meshless model for transient heat conduction analyses of 3D axisymmetric functionally graded solids*

Li Qing-Hua(李庆华), Chen Shen-Shen(陈莘莘)†, and Zeng Ji-Hui(曾骥辉)

*College of Civil Engineering, Hunan University of Technology, Zhuzhou* 412007, *China*

(Received 2 August 2013; revised manuscript received 21 August 2013)

A meshless numerical model is developed for analyzing transient heat conductions in three-dimensional (3D) axisymmetric continuously nonhomogeneous functionally graded materials (FGMs). Axial symmetry of geometry and boundary conditions reduces the original 3D initial-boundary value problem into a two-dimensional (2D) problem. Local weak forms are derived for small polygonal sub-domains which surround nodal points distributed over the cross section. In order to simplify the treatment of the essential boundary conditions, spatial variations of the temperature and heat flux at discrete time instants are interpolated by the natural neighbor interpolation. Moreover, the using of three-node triangular finite element method (FEM) shape functions as test functions reduces the orders of integrands involved in domain integrals. The semi-discrete heat conduction equation is solved numerically with the traditional two-point difference technique in the time domain. Two numerical examples are investigated and excellent results are obtained, demonstrating the potential application of the proposed approach.

**Keywords:** meshless method, transient heat conduction problem, axisymmetric, functionally graded materials, natural neighbor interpolation

**PACS:** 02.60.Cb, 02.60.Lj, 44.10.+i **DOI:** 10.1088/1674-1056/22/12/120204

## 1. Introduction

In recent years, functionally graded materials (FGMs) have been introduced and applied in the development of structural components subject to non-uniform service requirements. A key feature that distinguishes FGMs from homogeneous materials is that the thermal properties of the former vary spatially. Often, these spatial gradients in material behavior render FGMs superior to conventional composites.[1,2] Due to their excellent thermal properties, FGMs are expected to be used in the environments of high temperature and high heating rate. Accordingly, the determination of transient temperature field is an important topic for those advantageous materials and has received a considerable attention from researchers. However, because of the intrinsic complexity of the corresponding governing equation, analytical approaches for FGMs are restricted to simple geometry and boundary conditions.[2] As a result, numerical methods turn to be the only viable solution as no easier alternatives are available.

After more than half a century of development, the finite element method (FEM)[3] is now firmly accepted as a most powerful general technique for the numerical solution of a variety of problems encountered in engineering. Thus, the FEM has been developed over the past few decades to transient heat conduction analysis in FGMs.[4,5] However, in the case of complex geometries, the generation of highly distorted mesh is very common. Once the mesh used for the analysis has geometric distortions, the accuracy of the numerical results may drop off dramatically.[6] As another powerful alternative numerical tool, the boundary element method (BEM)[7] only requires the boundary of the problem to be discretized into elements. Nevertheless, the numerical implementation of the BEM requires fundamental solution and it is time-consuming and tedious to deal with various singular integrals. Therefore, except the work by Sutradhar *et al.*[8] the application of BEM to three-dimensional (3D) transient heat conduction analysis in FGMs has not been found in the published literature.

In the past two decades, more and more attention[9–12] has been paid to the development and application of meshless methods. In the meshless methods, no mesh is required to discretize the problem domain, and the approximate solution is constructed entirely based on a set of scattered nodes. Hence, some special advantages can be found from the problems which are difficult to solve by the conventional mesh-based methods.[13,14] Although most meshless methods originate from solid mechanics, a wide variety of literature is available on the application of meshless methods to heat conduction problems. The element-free Galerkin (EFG) method of solving composite heat transfer problems,[15] unsteady and nonlinear heat transfer problems[16,17] has been reported. However, the EFG method requires background cells to integrate a weak form over the entire domain or boundary of the problem. In order to alleviate the global integration background mesh, Atluri and Zhu[18] presented a new and innovative meshless approach in which Petrov–Galerkin weight functions instead

*Project supported by the National Natural Science Foundation of China (Grant No. 11002054) and the Foundation of Hunan Educational Committee (Grant No. 12C0059).

†Corresponding author. E-mail: chenshenshen@tsinghua.org.cn

© 2013 Chinese Physical Society and IOP Publishing Ltd 

of the traditional Galerkin weighted residual method is used. This method, referred to as the meshless local Petrov–Galerkin (MLPG) method, is a truly meshless method since it requires no elements or background cells, for either the interpolation or the integration purposes. By now, the MLPG method has been successfully used to solve heat conduction problems.[19–22] Although the MLPG method is an efficient meshless method, the essential boundary conditions cannot be enforced directly when the non-interpolative moving least squares (MLS) approximation is used. In order to overcome this difficulty, a series of MLPG-type methods based on different interpolative meshless shape functions have been proposed and successfully used to solve heat conduction problems.[23–25] Some other meshless methods have also been reported, such as those by Gao,[26] Cheng and Liew,[27] Peng and Cheng,[28] Skouras *et al.*[29]

In the present paper, we present an advanced computational method for transient heat conduction analysis in 3D axisymmetric continuously nonhomogeneous functionally graded materials (FGMs) using the meshless local natural neighbor interpolation (MLNNI) method, which is derived from the generalized meshless local Petrov–Galerkin (MLPG) method as a special case. The MLNNI method, originated from Cai and Zhu,[30] shows great promise since it can not only maintain prominent features of the MLPG method but also employ the advantage of easy imposition of essential boundary conditions of the natural neighbor interpolation (NNI).[31] A 3D axisymmetric body is created by the rotation of the cross section around the axis of symmetry. Axial symmetry of the geometry and boundary conditions reduces the original 3D initial-boundary value problem into a two-dimensional (2D) problem. A set of properly scattered nodes within the cross section is employed and no elements or meshes are required. The local weak form of partial differential equations (PDEs) is derived by the weighted residual method based on simple polygonal sub-domains. The spatial variations of the temperature and the heat flux are interpolated by the NNI, and test functions are taken as the three-node triangular FEM shape functions. The semi-discrete heat conduction equation is solved numerically with the traditional two-point difference technique in the time domain. In the end, two numerical examples are then provided to verify the validity and accuracy of the proposed method for transient heat conduction analysis of 3D axisymmetric functionally graded solids.

## 2. Governing equations

Consider a transient heat conduction problem for a nonhomogeneous medium in domain $\Omega$ bounded by $\Gamma$, the governing equation is[1]

$$T_{,ii}(\boldsymbol{x},t) - \frac{1}{\alpha(\boldsymbol{x})}\frac{\partial T(\boldsymbol{x},t)}{\partial t} + \frac{k_{,i}}{k}(\boldsymbol{x})T_{,i}(\boldsymbol{x},t) = -\frac{1}{k(\boldsymbol{x})}Q(\boldsymbol{x},t), \tag{1}$$

where $T(\boldsymbol{x},t)$ is the temperature field, $k$ and $\alpha$ are the thermal conductivity and diffusivity, respectively, $t$ is the time, and $Q(\boldsymbol{x},t)$ is the density of the body heat sources. Summation convention is applied to index $i$, which will cover either from 1 to 2 for 2D problems, or from 1 to 3 for 3D problems.

For an axisymmetric problem, it is convenient to use cylindrical coordinates, $(r,\varphi,z)$. In such a case the governing equation (1) can be rewritten into the following form:

$$(k(\boldsymbol{x})T_{,i}(\boldsymbol{x},t))_{,i} + \frac{k(\boldsymbol{x})}{r}\frac{\partial T(\boldsymbol{x},t)}{\partial r} + Q(\boldsymbol{x},t) = \frac{k(\boldsymbol{x})}{\alpha(\boldsymbol{x})}\frac{\partial T(\boldsymbol{x},t)}{\partial t}. \tag{2}$$

The initial conditions and the boundary conditions of the problem are

$$T(\boldsymbol{x},0) = T_0, \quad \text{in } \Omega, \tag{3a}$$

$$T(\boldsymbol{x},t) = \bar{T}(\boldsymbol{x},t), \quad \text{on } \Gamma_1, \tag{3b}$$

$$q(\boldsymbol{x},t) = k(\boldsymbol{x})T_{,i}(\boldsymbol{x})n_i(\boldsymbol{x}) = \bar{q}(\boldsymbol{x},t), \quad \text{on } \Gamma_2, \tag{3c}$$

where $\Gamma_1$ and $\Gamma_2$ are the Dirichlet boundary and the Neumann boundary, respectively, and $n_i$ are the components of the unit outward normal vector to the boundary $\Gamma$.

## 3. Numerical implementation of the MLNNI method

### 3.1. Brief description of the natural neighbor interpolation

In order to achieve a non-element-type interpolation, meshless methods each require a local interpolation or approximation to represent the trial function. The natural neighbor interpolation (NNI)[31] used in the present analysis may be considered as one of such schemes. The NNI is based on the well-known Voronoi diagram and Delaunay tessellation. Consider a set of nodes $N = \{\boldsymbol{x}_1, \boldsymbol{x}_2, \boldsymbol{x}_3, \ldots, \boldsymbol{x}_M\}$ in 2D Euclidean space $R^2$. The Voronoi diagram is a partition of the space into sub-regions $T_I$, where each region $T_I$ is associated with a node $\boldsymbol{x}_I$, such that any point $\boldsymbol{x}$ in $T_I$ is closer to node $\boldsymbol{x}_I$ than to any other nodes. In mathematical terms, the Voronoi polygon $T_I$ is defined as[32]

$$T_I = \left\{\boldsymbol{x} \in R^2 : d(\boldsymbol{x},\boldsymbol{x}_I) < d(\boldsymbol{x},\boldsymbol{x}_J)\forall J \neq I\right\}, \tag{4}$$

where $d(\boldsymbol{x},\boldsymbol{x}_I)$ is the distance between $\boldsymbol{x}$ and $\boldsymbol{x}_I$. Simply connecting the nodes whose Voronoi cells have common boundaries yields the Delaunay triangulation. The Voronoi diagram and its corresponding Delaunay triangulation are dual.

If an interpolation point $\boldsymbol{x}$ is tessellated along with the set of nodes $N$, then, in the newly constructed triangulation based on $N$ and $\boldsymbol{x}$, the natural neighbors of $\boldsymbol{x}$ are those nodes which

form an edge of a triangle with $\boldsymbol{x}$. The natural neighbor shape function of $\boldsymbol{x}$ with respect to a natural neighbor $I$ is defined as the ratio of the area of overlap of their Voronoi cells to the total area of the Voronoi cell of $\boldsymbol{x}$

$$\phi_I(\boldsymbol{x}) = A_I(\boldsymbol{x})/A(\boldsymbol{x}), \tag{5}$$

where

$$A(\boldsymbol{x}) = \sum_{J=1}^{n} A_J(\boldsymbol{x}), \tag{6}$$

and $n$ is the number of natural neighbors of the point $\boldsymbol{x}$. Referring to Fig. 1, $\boldsymbol{x}$ has four ($n=4$) natural neighbors (namely nodes 1–4) and the shape function $\phi_1(\boldsymbol{x})$ may be represented as

$$\phi_1(\boldsymbol{x}) = A_1/A_2, \tag{7}$$

where $A_1$ and $A_2$ denote the areas of quadrilateral $abfe$ and $abcd$, respectively.

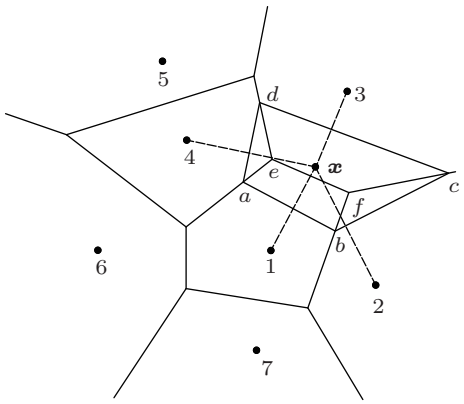



**Fig. 1.** The 1st-order and 2nd-order Voronoi cells about $\boldsymbol{x}$.

According to this definition, and in the context of two-dimensional approximations, the unknown temperature field $T(\boldsymbol{x})$ is approximated in the form

$$T(\boldsymbol{x}) = \sum_{I=1}^{n} \phi_I(\boldsymbol{x}) T_I, \tag{8}$$

where $T_I$ $(I = 1,2,\ldots,n)$ are the nodal temperatures of the $n$ natural neighbors. It should be stressed here that the natural neighbor (Sibson) shape functions possess some remarkable properties such as positivity, interpolation, partition of unity, and linear completeness.

### 3.2. Local weak-forms

In the implementation of the present MLNNI method, a weak form is first constructed over a set of overlapping local sub-domains $\Omega_{\rm s}^I$ $(I = 1,2,\ldots,M)$, where $I$ denotes a node, and $M$ is the total number of nodes. Using the local weighted residual technique, the local weak form of Eq. (2) over a local sub-domain $\Omega_{\rm s}^I$ can be written as

$$\int_{\Omega_{\rm s}^I} v\left(k(\boldsymbol{x})T_{,i}(\boldsymbol{x},t)\right)_{,i}\mathrm{d}\Omega + \int_{\Omega_{\rm s}^I} vQ(\boldsymbol{x},t)\mathrm{d}\Omega + \int_{\Omega_{\rm s}^I} v\frac{k(\boldsymbol{x})}{r}\frac{\partial T(\boldsymbol{x},t)}{\partial r}\mathrm{d}\Omega = \int_{\Omega_{\rm s}^I} v\frac{k(\boldsymbol{x})}{\alpha(\boldsymbol{x})}\frac{\partial T(\boldsymbol{x},t)}{\partial t}\mathrm{d}\Omega, \tag{9}$$

where $v$ is the test function. It should be stressed that there are neither Lagrange multipliers nor penalty parameters introduced in Eq. (9) because the essential boundary conditions can be imposed directly as in the FEM.

Using the relationship

$$v\left(k(\boldsymbol{x})T_{,i}(\boldsymbol{x},t)\right)_{,i} = \left(vk(\boldsymbol{x})T_{,i}(\boldsymbol{x},t)\right)_{,i} - v_{,i}k(\boldsymbol{x})T_{,i}(\boldsymbol{x},t) \tag{10}$$

and the divergence theorem in Eq. (9), we can obtain the following local symmetric weak formulation:

$$\begin{aligned}&\int_{\Gamma_{\rm s}^I} vk(\boldsymbol{x})T_{,i}(\boldsymbol{x},t)n_i\mathrm{d}\Gamma - \int_{\Omega_{\rm s}^I} v_{,i}k(\boldsymbol{x})T_{,i}(\boldsymbol{x},t)\mathrm{d}\Omega \\ &+ \int_{\Omega_{\rm s}^I} vQ(\boldsymbol{x},t)\mathrm{d}\Omega + \int_{\Omega_{\rm s}^I} v\frac{k(\boldsymbol{x})}{r}\frac{\partial T(\boldsymbol{x},t)}{\partial r}\mathrm{d}\Omega \\ =& \int_{\Omega_{\rm s}^I} v\frac{k(\boldsymbol{x})}{\alpha(\boldsymbol{x})}\frac{\partial T(\boldsymbol{x},t)}{\partial t}\mathrm{d}\Omega,\end{aligned} \tag{11}$$

where $\Gamma_{\rm s}^I$ is the boundary for the sub-domain $\Omega_{\rm s}^I$. When there is an intersection between the local boundary $\Gamma_{\rm s}^I$ and the global boundary $\Gamma$, the boundary $\Gamma_{\rm s}^I$ is usually composed of three parts: the internal boundary $\Gamma_{\rm si}^I$, the boundaries $\Gamma_{\rm s1}^I$ and $\Gamma_{\rm s2}^I$ over which the Dirichlet and Neumann conditions are used respectively. If there is no intersection between $\Gamma_{\rm s}^I$ and global boundary $\Gamma$, then $\Gamma_{\rm si}^I = \Gamma_{\rm s}^I$. Substituting Eq. (3c) into Eq. (11), the first term on the left-hand side of Eq. (11) becomes

$$\begin{aligned}&\int_{\Gamma_{\rm s}^I} vk(\boldsymbol{x})T_{,i}(\boldsymbol{x},t)n_i\mathrm{d}\Gamma \\ =& \int_{\Gamma_{\rm si}^I} vk(\boldsymbol{x})T_{,i}(\boldsymbol{x},t)n_i\mathrm{d}\Gamma + \int_{\Gamma_{\rm s1}^I} vk(\boldsymbol{x})T_{,i}(\boldsymbol{x},t)n_i\mathrm{d}\Gamma \\ &+ \int_{\Gamma_{\rm s2}^I} v\bar{q}\mathrm{d}\Gamma.\end{aligned} \tag{12}$$

In the present MLNNI method, as trial functions are constructed by the NNI, it is natural to construct polygonal sub-domain $\Omega_{\rm s}^I$ using the Delaunay tessellations. Therefore the polygonal sub-domain $\Omega_{\rm s}^I$ is constructed by collecting all the surrounding Delaunay triangles $T_{iI}$ with node $\boldsymbol{x}_I$ being their common vertices as shown in Fig. 2. By choosing the test function $v$ to be the three-node triangular FEM shape function $N_I$ in each Delaunay triangle $T_{iI}$ belonging to the sub-domain $\Omega_{\rm s}^I$, equation (12) can be simplified into

$$\begin{aligned}&\int_{\Gamma_{\rm s}^I} N_I k(\boldsymbol{x})T_{,i}(\boldsymbol{x},t)n_i\mathrm{d}\Gamma \\ =& \int_{\Gamma_{\rm s1}^I} N_I k(\boldsymbol{x})T_{,i}(\boldsymbol{x},t)n_i\mathrm{d}\Gamma + \int_{\Gamma_{\rm s2}^I} N_I\bar{q}\mathrm{d}\Gamma.\end{aligned} \tag{13}$$

As shown in Fig. 3, the integrals over $\Gamma_{\rm s1}^I$ in Eq. (13) can be divided into two cases. For Fig. 3(a), the test function $N_I$ is

equal to zero over the local prescribed boundary $\Gamma_{s1}^I$ and therefore the integral over $\Gamma_{s1}^I$ will vanish. For Fig. 3(b), as already pointed out, essential boundary conditions must be enforced on node $\boldsymbol{x}_I$ and therefore the integral over $\Gamma_{s1}^I$ in Eq. (13) does not need computing. Accordingly, equation (13) can be further simplified into

$$\int_{\Gamma_s^I} vk(\boldsymbol{x})T_{,i}(\boldsymbol{x},t)n_i \mathrm{d}\Gamma = \int_{\Gamma_{s2}^I} v\bar{q}\mathrm{d}\Gamma. \tag{14}$$

Then the substitution of Eq. (14) into Eq. (11) results in the following equation

$$\begin{aligned} &\int_{\Omega_s^I} N_I \frac{k(\boldsymbol{x})}{\alpha(\boldsymbol{x})}\frac{\partial T(\boldsymbol{x},t)}{\partial t}\mathrm{d}\Omega + \int_{\Omega_s^I} N_{I,i}k(\boldsymbol{x})T_{,i}(\boldsymbol{x},t)\mathrm{d}\Omega \\ &- \int_{\Omega_s^I} N_I \frac{k(\boldsymbol{x})}{r}\frac{\partial T(\boldsymbol{x},t)}{\partial r}\mathrm{d}\Omega \\ &= \int_{\Gamma_{s2}^I} N_I\bar{q}\mathrm{d}\Gamma + \int_{\Omega_s^I} N_I Q(\boldsymbol{x},t)\mathrm{d}\Omega. \end{aligned} \tag{15}$$

For the transient heat conduction problem, temperature $T$ is a function of both the spatial coordinates and time $t$. In this paper, we first discretize the space domain at an arbitrary time $t$. Assume that the problem domain $\Omega$ is represented by properly scattered nodes. By using the natural neighbour interpolation described in Subsection 3.1, the unknown temperature $T$ in Eq. (15) can be expressed as follows:

$$T(\boldsymbol{x},t) = \sum_{I=1}^{n} \phi_I(\boldsymbol{x})T_I(t). \tag{16}$$

The substitution of Eq. (16) into the weak form (15) for all nodes leads to the following discretized system equation:

$$\boldsymbol{C}\dot{\boldsymbol{T}}(t) + \boldsymbol{K}\boldsymbol{T}(t) = \boldsymbol{P}(t), \tag{17}$$

where

$$C_{IJ} = \int_{\Omega_s^I} \frac{k(\boldsymbol{x})}{\alpha(\boldsymbol{x})} N_I\phi_J \mathrm{d}\Omega, \tag{18a}$$

$$\begin{aligned} K_{IJ} = &\int_{\Omega_s^I} k(\boldsymbol{x})\left(\frac{\partial N_I}{\partial r}\frac{\partial \phi_J}{\partial r} + \frac{\partial N_I}{\partial z}\frac{\partial \phi_J}{\partial z}\right)\mathrm{d}\Omega \\ &- \int_{\Omega_s^I} \frac{N_I k(\boldsymbol{x})}{r}\frac{\partial \phi_J}{\partial r}\mathrm{d}\Omega, \end{aligned} \tag{18b}$$

$$P_I(t) = \int_{\Omega_s^I} N_I Q(\boldsymbol{x},t)\mathrm{d}\Omega + \int_{\Gamma_{s2}^I} N_I\bar{q}(\boldsymbol{x},t)\mathrm{d}\Gamma, \tag{18c}$$

$$\boldsymbol{T} = \big(T_1(t),\ T_2(t),\ \ldots,\ T_N(t)\big)^{\mathrm{T}}, \tag{18d}$$

$$\dot{\boldsymbol{T}} = \left(\frac{\partial T_1(t)}{\partial t},\ \frac{\partial T_2(t)}{\partial t},\ \ldots,\ \frac{\partial T_N(t)}{\partial t}\right)^{\mathrm{T}}, \tag{18e}$$

where $N$ is the total number of nodes in the entire domain. It should be noted here that the heat capacity matrix $\boldsymbol{C}$ and the heat conduction matrix $\boldsymbol{K}$ are both independent of time $t$.

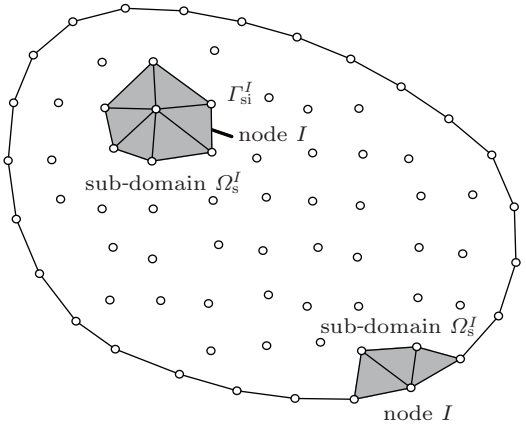



**Fig. 2.** Local polygonal sub-domain and boundary for node $I$.

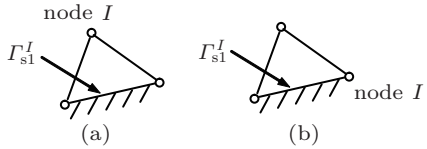



**Fig. 3.** Dirichlet boundary condition $\Gamma_{s1}^I$ over sub-domain $\Omega_s^I$.

### 3.3. Solution techniques

Equation (17) is a linear system of ordinary differential equations, in which time is the only independent variable. In this paper, we use the traditional two-point difference technique[23] for time discretization. The relation between $T_{t+\Delta t}$ and $T_t$ employed here can be written as follows:

$$\theta\left(\frac{\partial T}{\partial t}\right)_{t+\Delta t} + (1-\theta)\left(\frac{\partial T}{\partial t}\right)_t = \frac{T_{t+\Delta t} - T_t}{\Delta t}, \tag{19}$$

where $\Delta t$ represents the time step.

Solving Eq. (17) for $(\partial T/\partial t)_{t+\Delta t}$ and $(\partial T/\partial t)_t$, respectively, and substituting the results into Eq. (19), we can obtain

$$\begin{aligned} &(\boldsymbol{C}/\Delta t + \theta\boldsymbol{K})\boldsymbol{T}_{t+\Delta t} \\ &= (\boldsymbol{C}/\Delta t - (1-\theta)\boldsymbol{K})\boldsymbol{T}_t + \theta\boldsymbol{P}_{t+\Delta t} + (1-\theta)\boldsymbol{P}_t, \end{aligned} \tag{20}$$

where $\theta$ is the time weighted coefficient. By changing the value of $\theta$ from 0 to 1, different members of this family of methods are identified. In the present paper, $\theta = 2/3$ is chosen, which corresponds to the Galerkin form.

## 4. Numerical examples

With the purpose of validating the proposed technique, two numerical examples are presented to perform transient heat conduction analysis of 3D axisymmetric functionally graded solids in this section. Three Gaussian points are used in each Delaunay triangular region for domain integrals unless otherwise mentioned.

### 4.1. Full cylinder

The first example is to examine an infinitely long full cylinder with a radius $a = 1$ m loaded by a thermal shock with the Heaviside time step variation $T(a,t) = T_0 H(t-0)$ where $T_0 = 100$ °C as depicted in Fig. 4. The same problem was also analyzed by Sladek *et al.*[1] using the local BIEM.

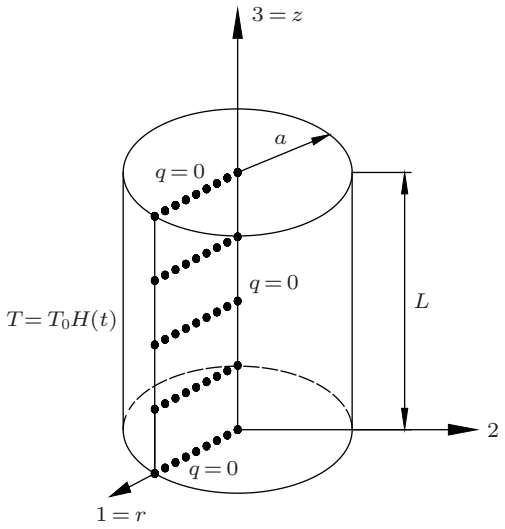



**Fig. 4.** Boundary conditions and node distribution in analyzed domain for a finite full cylinder.

In order to check the accuracy of the proposed method, homogeneous material properties are assumed in the first step. The diffusivity coefficient is chosen to be $\alpha = 1.0\ \mathrm{m}^2 \cdot \mathrm{s}^{-1}$. We can consider a finite part of the cylinder in the numerical analysis, with heat fluxes vanishing on both artificial cross sections of the cylinder due to the fact that boundary conditions along the cylinder are uniform. The cylinder can be created by rotating a rectangular plate of height $L$ and width $a$ about the $z$ axis as shown in Fig. 4. Here, $L = 1$ m is chosen. In the computation, 45 $(5 \times 9)$ nodes distributed in 5 layers in the $z$ axis direction, each layer having 9 nodes equidistantly distributed in the radial direction, are employed. The time step used in the two-point difference technique is $\Delta t = 0.02$ s. The analytical solution for this problem is known as[33]

$$T(r,t) = T_0 - \frac{2T_0}{a} \sum_{n=1}^{\infty} \frac{\mathrm{J}_0(r\beta_n)}{\beta_n \mathrm{J}_1(a\beta_n)} \exp(-\alpha\beta_n^2 t), \qquad (21)$$

where $\beta_n$ are the roots of the following transcendental equation

$$\mathrm{J}_0(a\beta_n) = 0. \qquad (22)$$

In Fig. 5, computational time history results for the temperature on the axis of the cylinder, obtained by the present MLNNI method, are depicted. For comparison, the analytical results for the temperature on the axis of the cylinder are also plotted in the same graph. From Fig. 5, one can observe that the present method produces a result indistinguishable from the analytical solution.

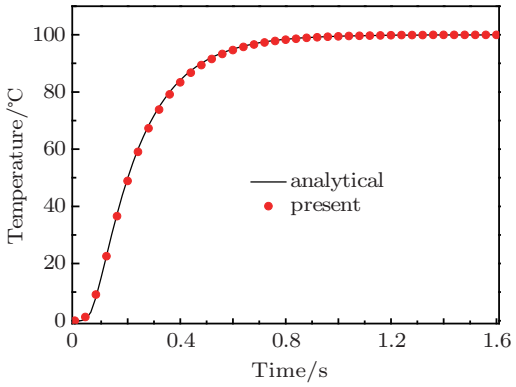



**Fig. 5.** (color online) Time variations of the temperature on the axis of a homogeneous cylinder.

Next we proceed to consider a functionally graded full cylinder with the thermal conductivity and diffusivity being graded in the radial direction $r$ as described by

$$k(\boldsymbol{x}) = k_0 \mathrm{e}^{\gamma r}, \quad \alpha(\boldsymbol{x}) = \alpha_0 \mathrm{e}^{\gamma r}, \qquad (23)$$

with $k_0 = 1.0\ \mathrm{W} \cdot \mathrm{m}^{-1} \cdot \mathrm{deg}^{-1}$, $\alpha_0 = 1.0\ \mathrm{m}^2 \cdot \mathrm{s}^{-1}$, and $\gamma$ is known as the exponential parameter. Here $\gamma = 0$ corresponds to a homogeneous material with constant thermal conductivity $k_0$ and diffusivity $\alpha_0$. For three different exponential parameters $\gamma = 0$, $-1$, and $-2\ \mathrm{m}^{-1}$, numerical results for the time variation of the temperature on the axis of the cylinder, are shown in Fig. 6. It is clear that the temperature evolution for a homogeneous cylinder with $\gamma = 0$ is steeper than that for the functionally graded cylinder with the decreasing of thermal parameters along radial coordinate.

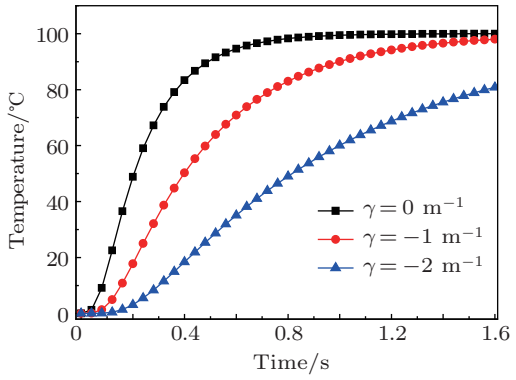



**Fig. 6.** (color online) Time variations of the temperature on the axis of a functionally graded full cylinder.

### 4.2. Hollow cylinder

The second example is an infinitely long functionally graded thick-walled hollow cylinder with the radii $a = 8 \times 10^{-2}$ m and $b = 10 \times 10^{-2}$ m as depicted in Fig. 7. Since boundary conditions along the cylinder are considered to be uniform a finite part of the cylinder in the numerical analysis is selected with length $L = 2 \times 10^{-2}$ m. On the external surface of the hollow cylinder the temperature, $T = 1$ °C, is prescribed either stationarily or as Heaviside time-step thermal loading at

time instant $t = 0$. The inner surface is kept at zero temperature. All the other surfaces are insulated. For comparison purpose, a homogeneous material is first considered. The analytical solution for the homogeneous material can be written as[33]

$$T(r,t) = \frac{\ln(r/a)}{\ln(b/a)} - \pi \sum_{n=1}^{\infty} \frac{J_0^2(a\beta_n)U_0(r\beta_n)}{J_0^2(a\beta_n) - J_0^2(b\beta_n)} \times \exp(-\alpha\beta_n^2 t), \quad (24)$$

where

$$U_0(r\beta_n) = J_0(r\beta_n)Y_0(b\beta_n) - J_0(b\beta_n)Y_0(r\beta_n) \quad (25)$$

and $\beta_n$ are roots of the following transcendental equation:

$$J_0(ar)Y_0(br) - J_0(br)Y_0(ar) = 0, \quad (26)$$

with $J_0(r)$ and $Y_0(r)$ being Bessel functions of first and second kind and zeroth order respectively.

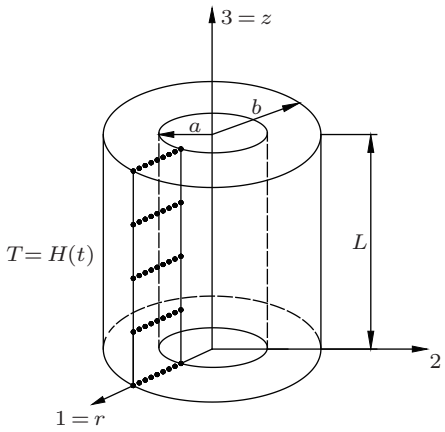



**Fig. 7.** Boundary conditions and node distribution in analyzed domain for a finite hollow cylinder.

In our numerical calculations, we assume an exponential spatial variation for both the thermal conductivity and diffusivity, i.e.,

$$k = k_0 e^{\gamma(r-a)}, \quad \alpha = \alpha_0 e^{\gamma(r-a)}, \quad (27)$$

where $k_0 = 17\ \mathrm{W \cdot m^{-1} \cdot deg^{-1}}$, and $\alpha_0 = 0.17 \times 10^{-4}\ \mathrm{m^2 \cdot s^{-1}}$. The time step used in two-point difference technique is $\Delta t = 0.5$ s. As shown in Fig. 7, the node distribution consisting of 45 $(9 \times 5)$ nodes uniformly distributed in the rectangular domain with 9 nodes in the radial direction is employed. Figure 8 depicts the time variations of temperature at the radius $r = 9$ cm for the homogeneous case with constant thermal conductivity ($k_0$) and diffusivity ($\alpha_0$). Again, the MLNNI method gives good agreement with the analytical solutions. It is also observed that the temperature field approaches to steady state after $t = 15$ s. In addition, figure 9 shows the variations of the temperature with the radial coordinate at four different time instants.

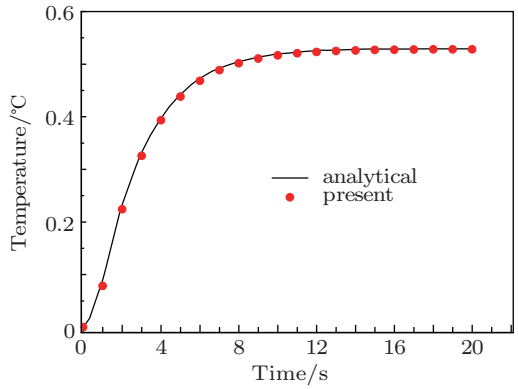



**Fig. 8.** (color online) Time variations of the temperature at $r = 9.0$ cm in the hollow cylinder with homogeneous material properties.

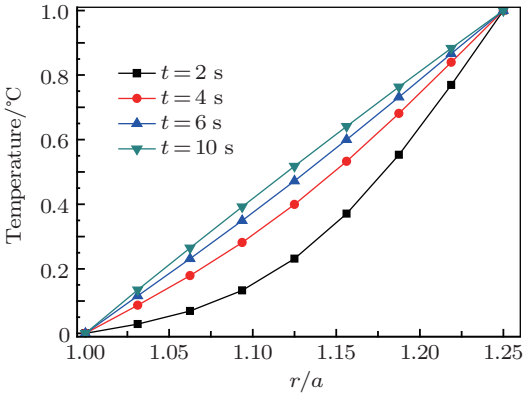



**Fig. 9.** (color online) Temperature variations with radial coordinate $r$ at different time levels for a hollow cylinder with homogeneous material properties.

To investigate the influence of the material gradation on the temperature variation, two different exponential parameters $\gamma = 0.2\ \mathrm{cm^{-1}}$ and $0.5\ \mathrm{cm^{-1}}$ are chosen in numerical calculation of the FGMs and the results are compared with the results of the homogeneous material. The time variations of the temperature at $r = 9$ cm for three values of the exponential parameter $\gamma$ are shown in Fig. 10. In addition, the steady-state temperature profiles along the radial direction are plotted in Fig. 11 for four different exponential parameters. One can observe from Figs. 10 and 11 that the increasing of the exponential parameter of FGMs raises the spatial variation of the temperature response.

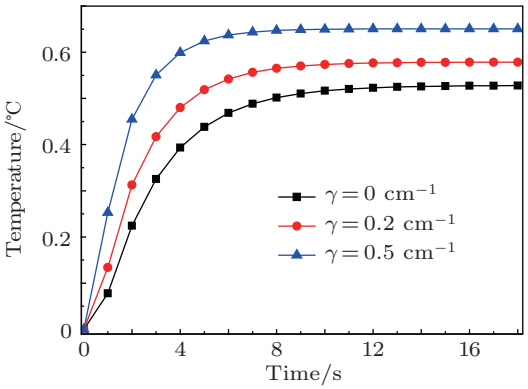



**Fig. 10.** (color online) Time variations of the temperature at $r = 9.0$ cm in a functionally graded hollow cylinder.

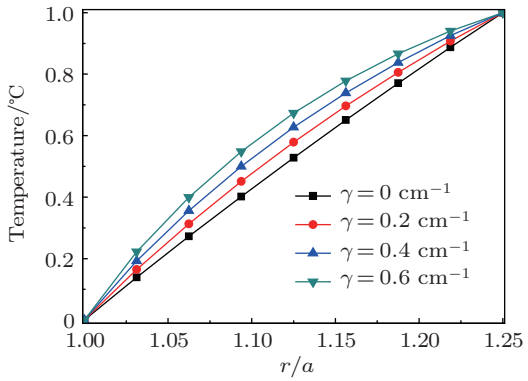



**Fig. 11.** (color online) Steady state temperature distributions along the radial direction for a functionally graded hollow cylinder.

## 5. Conclusions

In recent years, meshless methods have gained significant popularity due to their advantages in some practical applications. In addition, the understanding of temperature distribution and relevant heat fluxes in FGMs under severe thermal environment is important for several industrial applications. Motivated by the need to extend the applications of the newly developed numerical method, we propose a solution procedure based on the MLNNI for transient heat conduction analysis in 3D axisymmetric functionally graded bodies with continuously nonhomogeneous material properties. In the MLNNI method, the NNI and the three-node triangular FEM shape function are chosen differently as trial function and test function. Since the shape functions constructed by the NNI possess delta function property, the essential boundary conditions can be implemented directly. In addition, the construction of the polygonal local sub-domain for each node is very simple with the help of the Delaunay tessellation. Time integration of the semi-discrete heat conduction equation is achieved by using the traditional two-point difference technique. Some test problems are studied by the proposed scheme, and the obtained results are compared with other available solutions. It is shown that they are in complete agreement with each other and the proposed solution technique is quite efficient.

## References


[1] Sladek J, Sladek V, Krivacek J and Zhang C 2003 *Comput. Mech.* **32** 169

[2] Sladek J, Sladek V, Hellmich Ch and Eberhardsteiner J 2007 *Comput. Mech.* **39** 323

[3] Wang X C 2003 *Finite Element Method* (Beijing: Tsinghua University Press) (in Chinese)

[4] Kim J H and Paulino G H 2002 *J. Appl. Mech.* **69** 502

[5] Wang B L, Mai Y W and Zhang X H 2004 *Acta Materialia* **52** 4961

[6] Cen S, Fu X R and Zhou M J 2011 *Comput. Methods Appl. Mech. Eng.* **200** 2321

[7] Gao X W and Davies T G 2000 *Int. J. Solids Struct.* **37** 4987

[8] Sutradhar A, Paulino G H and Gray L J 2002 *Eng. Anal. Bound. Elem.* **26** 119

[9] Li X L, Zhu J L and Zhang S G 2009 *Eng. Anal. Bound. Elem.* **33** 1273

[10] Li X L 2011 *Int. J. Numer. Meth. Eng.* **88** 442

[11] Cheng Y M and Peng M J 2005 *Sci. China Ser. G: Phys. Mech. Astron.* **48** 641

[12] Cheng Y M and Li J H 2006 *Sci. China Ser. G: Phys. Mech. Astron.* **49** 46

[13] Feng Z, Wang X D and Ouyang J 2013 *Chin. Phys. B* **22** 074704

[14] Li X L and Li S L 2013 *Chin. Phys. B* **22** 080204

[15] Singh I V and Tanaka M 2006 *Comput. Mech.* **38** 521

[16] Singh A, Singh I V and Prakash R 2006 *Int. J. Heat Mass Transfer* **33** 231

[17] Singh A, Singh I V and Prakash R 2006 *Numer. Heat Transfer Part A* **50** 125

[18] Atluri S N and Zhu T 1998 *Comput. Mech.* **22** 117

[19] Sladek J, Sladek V and Hon Y C 2006 *Eng. Anal. Bound. Elem.* **30** 650

[20] Sladek J, Sladek V, Tan C L and Atluri S N 2008 *Comput. Model Eng. Sci.* **32** 161

[21] Wu X H and Tao W Q 2008 *Int. J. Heat Mass Transfer* **51** 3103

[22] Wang Q F, Dai B D and Li Z F 2013 *Chin. Phys. B* **22** 080203

[23] Chen L and Liew K M 2011 *Comput. Mech.* **47** 455

[24] Li Q H, Chen S S and Kou G X 2011 *J. Comput. Phys.* **230** 2736

[25] Dai B D, Zheng B J, Liang Q X and Wang L H 2013 *Appl. Math. Comput.* **219** 10044

[26] Gao X W 2006 *Int. J. Numer. Method Eng.* **66** 1411

[27] Cheng R J and Liew K M 2009 *Comput. Mech.* **45** 1

[28] Peng M J and Cheng Y M 2009 *Eng. Anal. Bound. Elem.* **33** 77

[29] Skouras E D, Bourantas G C, Loukopoulos V C and Nikiforidis G C 2011 *Eng. Anal. Bound. Elem.* **35** 452

[30] Cai Y C and Zhu H H 2004 *Eng. Anal. Bound. Elem.* **28** 607

[31] Sukumar N, Moran B and Belytschko T 1998 *Int. J. Numer. Method Eng.* **43** 839

[32] Green P J and Sibson R R 1978 *Comput. J.* **21** 168

[33] Carslaw H S and Jaeger J C 1959 *Conduction of Heat in Solids* (Oxford: Clarendon Press)